

2014-11

# Chitosan does not inhibit enzymatic action of human pancreatic lipase in Langmuir monolayers of 1,2-didecanoyl-glycerol (DDG)

Colloids and Surfaces B,Amsterdam : Elsevier BV,v. 123, p. 870-877, Nov. 2014
http://www.producao.usp.br/handle/BDPI/50593

Colloids and Surfaces B: Biointerfaces 123 (2014) 870–877

Contents lists available at ScienceDirect

Colloids and Surfaces B: Biointerfaces

journal homepage: www.elsevier.com/locate/colsurfb

# Chitosan does not inhibit enzymatic action of human pancreatic lipase in Langmuir monolayers of 1,2-didecanoyl-glycerol (DDG)

Adriano L. Souza[a,*], Felippe J. Pavinatto[a], Luciano Caseli[b], Diogo Volpati[a], Paulo B. Miranda[a], Osvaldo N. Oliveira Jr.[a]

[a] São Carlos Institute of Physics, University of São Paulo (USP), PO Box 369, São Carlos, SP 13566-590, Brazil
[b] Institute for Environmental, Chemical and Pharmaceutical Sciences, Federal University of São Paulo (UNIFESP), Diadema, SP 09972-270, Brazil

ARTICLE INFO

*Article history:*
Received 7 July 2014
Received in revised form 13 October 2014
Accepted 16 October 2014
Available online 28 October 2014

*Keywords:*
Chitosan
Fat reduction
Human pancreatic lipase
Langmuir monolayers
Sum-frequency generation spectroscopy

ABSTRACT

In this study, we tested the hypothesis according to which chitosan reduces lipid digestion by blocking the access of lipases to ingested fat. Because lipase action takes place mostly at interfaces, we produced Langmuir films of 1,2-didecanoyl-glycerol (DDG), which is the substrate for human pancreatic lipase (HPL). The experimental assays were carried out in acidic medium, at pH 3.0, to ensure that chitosan is completely soluble. Chitosan was found to affect strongly the surface activity of HPL that forms a Gibbs monolayer at the air/water interface, but did not inhibit the enzymatic action of HPL toward the DDG monolayer. The latter was observed using two surface-specific spectroscopic techniques, namely polarization-modulated infrared reflection–absorption and sum-frequency generation (SFG). The extension of DDG hydrolysis calculated using SFG spectroscopy was 33% in the absence of chitosan, and ranged from 29 to 50% in the presence of chitosan at concentrations of 0.20 g $L^{-1}$ and 0.30 g $L^{-1}$, respectively. Therefore, fat "protection" by chitosan is unlikely to be an important factor in fat reduction.



## 1. Introduction

Chitosans have been extensively used for a number of applications, including as a matrix for the immobilization of functional materials in nanostructured films [1] and in nutrition [2] and medicine [3] owing to their suitable properties. For they are biocompatible, biodegradable and non-toxic, thus being amenable to use in tissue engineering, artificial skin, microspheres for drug delivery systems, nanoparticles as protein carriers, antibacterial agent and as weight loss or fat absorption reducer [4–6]. Commercially available chitosans are found in tablets as food supplement [7], especially with the promise of weight loss *via* reduced fat absorption. However, their efficacy for weight loss is highly controversial, and in a survey of the literature reports are found for both confirmation and denial of this property. Conflicting results were obtained in *in vivo* experiments with humans and mice where chitosan was used as supplement in diets, with no or very little weight loss in some studies [8–12], whereas in other studies chitosan was able to inhibit increases in body weight [13,14].

In spite of the controversy over the efficacy in weight loss, attempts have been made to understand how chitosan would act in reducing fat. As in practically all other applications of chitosans, the molecular-level mechanisms to explain the action are lacking, even in the cases where the chitosan activity has been proven beyond doubt, as in the bactericide property. Three mechanisms have been proposed to explain chitosan action as possible fat reducer. They were based on *in vivo* experiments made with humans [15] and *in vitro* experiments using solutions [16], microemulsions [17] and emulsions [18]: (i) chitosan binds to bile acids making them unavailable to emulsify the fat ingested [15], thus leading to inadequate processing of fat for lipase digestion; (ii) chitosan acts as an alternative substrate for lipases, which causes less fat absorption by simple competition between these possible targets for the lipases [16]; (iii) chitosan encapsulates fat floccules [17,18], and in contrast to the latter hypothesis (ii), it should be a barrier for the lipases, thus limiting their access to the fat.

Fat digestion is performed by lipases, which are enzymes that catalyze the hydrolysis reaction of acylglycerides producing fatty acids. This reaction is enhanced at interfaces due to interfacial activity by most lipases [19]. Therefore, bile salts, proteins and surfactants were able to inhibit lipases enzymatic activity by hindering their adsorption to the interface [20–23]. Human pancreatic lipase (HPL) has been inhibited by tetrahydrolipstatin (orlistat) with a larger effect in the presence of bile salts [24,25]. An even more potent inhibitor than orlistat was ε-polylysine, which modified the activity of pancreatic lipase of mice [26]. Grove et al.

* Corresponding author. Tel.: +55 01633739797234; fax: +55 01633715365.
*E-mail address:* adriano.lsouza@yahoo.com.br (A.L. Souza).

http://dx.doi.org/10.1016/j.colsurfb.2014.10.040
0927-7765/

[27] found that epigallocathechin-3-gallate inhibited this lipase. Porcine pancreatic lipase had its enzymatic activity inhibited in olive oil emulsions containing galactolipid digalactosyldiacylglycerol (DGDG) [28], while a mixed monolayer of DGDG/bile salts hampered porcine pancreatic lipase/colipase adsorption to the interface by steric hindrance of galactosyl groups [29]. Triacylglycerols have been also found to inhibit lipases [30].

Monolayers at the air–water interface provide an important methodology to investigate hydrolysis of lipids by lipases [31]. With the technique referred to as "zero order" trough [32], the enzymatic reaction is independent of the lipid concentration, from which a kinetic parameter may be inferred. Hydrolysis at air–liquid interfaces has been also monitored in phospholipases by polarization-modulated infrared absorption reflection spectroscopy (PM-IRRAS), where stretching bands of functional groups can be monitored as a function of reaction time [33–37]. As far as chitosans are concerned, Langmuir monolayers have been used to mimic the interaction with biological membrane models and for immobilizing enzymes [38] to prepare biosensors [39]. Incidentally, the Langmuir–Blodgett technique is useful in the study of molecular-level interactions, in addition to allowing for assembling nanomaterials for sensors and optical and electronic devices [40,41]. Chitosan was able to expand and penetrate phospholipid Langmuir monolayers [42–45]. Two main representative phospholipids used were phosphatidylglycerol and phosphatidylcholine to mimic bacterial and mammalian membranes [46–48], respectively. Other components employed in monolayers included stearic acid and cholesterol [49–51]. From these studies, one can infer that the positively charged chitosans interact more strongly with negatively charged phospholipids, though hydrophobic interactions also play an important role [52,53].

In this paper, we test the hypothesis of chitosan affecting the activity of human pancreatic lipase (HPL) in Langmuir monolayers of 1,2–didecanoyl-*sn*-glycerol (DDG). DDG was chosen because it is the substrate for HPL action, while the choice of HPL was based on the fact that it catalyzes *ca.* 70% of lipid hydrolysis [20]. In addition to surface pressure isotherms to probe adsorption of chitosan on DDG monolayers, we used two surface-specific vibrational spectroscopic techniques, namely PM-IRRAS and Sum-Frequency Generation (SFG), to study the hydrolysis of DDG by HPL. An acidic medium was employed in this study to guarantee chitosan solubility. Though the optimum pH for HPL action is higher, there is evidence from the literature that its catalytic activity at pH 3.0 is still significant [54].

## 2. Materials and methods

### 2.1. Materials

1,2-Didecanoyl-*sn*-glycerol (DDG) and human pancreatic lipase (HPL) (BCR-693 1EA) were purchased from Avanti Polar Lipids and Sigma–Aldrich respectively, and used as received. Chitosan was purchased from Galena Farmacêutica (Brazil) with a degree of acetylation of 19% and molecular weight of 113,000 Da. Before use, chitosan was purified by dissolution in HCl 0.10%, precipitated in a solution of NaOH, filtered and washed with water and ethanol until complete neutrality. NaOH, boric acid, citric acid, phosphoric acid and HCl were purchased from Synth and used as received. Water used in all experiments was purified by a Millipore System and had resistivity of 18.2 MΩ cm. A Theorell–Stenhagen buffer at pH 3.0 was used to prepare chitosan solutions, which were employed as aqueous subphases for Langmuir monolayers. The buffer was prepared by dissolving NaOH, boric acid, citric acid and phosphoric acid in water, while pH was adjusted to 3.0 by adding HCl aqueous solution in a concentration of 2.0 mol $L^{-1}$.

### 2.2. Methodology

DDG Langmuir monolayers were prepared in a KSV mini trough (KSV, Finland) housed in a class 10,000 clean room. The surface pressure sensor was based on the Wilhelmy method using a filter paper. DDG was spread at concentration of $1.2 \times 10^{-3}$ mol $L^{-1}$ in chloroform on the surface of the aqueous subphases containing chitosan solutions in concentrations varying from 0.05 to 0.30 g $L^{-1}$. Surface pressure-area isotherms were obtained by compressing the monolayers with movable barriers at a rate of 10 mm $min^{-1}$ (trough dimensions 75 mm × 323 mm). The temperature was maintained at 20 ± 1 °C. Compressional modulus ($C_S^{-1}$), also known as equilibrium in-plane elasticity, was calculated for the monolayers and it is defined as $-A(\partial\pi/\partial A)_T$, where $A$ is the mean molecular area and $\pi$ is the surface pressure. Adsorption kinetics curves of HPL were obtained using a Kibron tensiometer (Micro Trough X). The experiments were carried out with a Theorell–Stenhagen buffer at pH 3.0 and chitosan solutions in concentrations of 0.20 and 0.30 g $L^{-1}$. The well of the trough was filled with Theorell–Stenhagen buffer or chitosan solution and 10 μL of HPL solution prepared with the Theorell–Stenhagen buffer. The final concentration of HPL in each case was 1.4 μg $mL^{-1}$ and the change in surface pressure was monitored as a function of time.

Polarization-modulated infrared reflection absorption spectroscopy (PM-IRRAS) experiments were performed using a KSV PMI550 instrument (KSV, Finland). The light beam reached the monolayer with an incidence angle of 81°. Since the incident radiation was modulated between *s* and *p* polarizations at high frequency and the spectra were obtained in both polarizations simultaneously, the effect of the water vapor was reduced. The difference between the *s* and *p* spectra provides information on species present at the interface while the sum is the reference spectrum. Experiments were performed in DDG monolayers in the presence and absence of chitosan with the surface pressure at 30 mN $m^{-1}$, which is the value corresponding to cell membranes in *in vivo* experiments [55]. When the surface pressure reached 30 mN $m^{-1}$, 5.0 mL of a 0.070 g $L^{-1}$ HPL stock solution was injected behind the barrier. The final HPL concentration of 1.4 μg $mL^{-1}$ was the same used in experiments of adsorption kinetics in the Kibron tensiometer. The resolution of the spectra was 8 $cm^{-1}$.

Sum-frequency generation (SFG) measurements were used to probe the interfacial interaction between DDG and subphase constituents, and to estimate DDG hydrolysis by HPL, including the influence from chitosan in this process. SFG is a second-order nonlinear optical process intrinsically specific to interfaces, since the generation of a sum-frequency signal is forbidden in media that present inversion symmetry. Consequently, the SFG signal arises only from molecules adsorbed at interfaces, where the inversion symmetry is broken. However, if the adsorbed molecules have a random orientation, the SFG signal also vanishes. Therefore, even at interface the molecules must have a net average orientation to yield a measurable SFG signal [56]. The experimental setup is based on a commercial spectrometer (Ekspla, Lithuania) equipped with a pulsed $Nd^{3+}$:YAG laser (28 ps pulse duration, 20 Hz repetition rate), a harmonic-generation unit and an optical parametric amplifier with a difference frequency stage that generates an infrared (IR) beam tunable from 1000 to 4000 $cm^{-1}$ with pulse energy varying from ~30 to 200 μJ within this tuning range. The visible beam ($\omega_{vis}$) was split from the harmonic unit (532 nm, ~700 μJ/pulse) and overlapped spatially and temporally with the tunable mid-infrared beam ($\omega_{IR}$) at the interface, giving rise to an emitted sum-frequency signal ($\omega_{SFG} = \omega_{vis} + \omega_{IR}$) that is measured by a photomultiplier after spatial and spectral filtering. The spot sizes and incidence angles for the IR and visible beams are (0.50 mm, 55°) and (1.00 mm, 60°), respectively. Scanning the frequency of the infrared beam, when it coincides with the frequency of a normal vibration of adsorbed

molecules, the intensity of the SFG signal resonantly increases, yielding their vibrational spectrum. The SFG signal was collected for each scan with 100 shots per data point and a 3 $cm^{-1}$ resolution.

The intensity of the SFG signal is proportional to the square of the effective second-order susceptibility of the interface, $\chi^{(2)}_{eff}$, which may be expressed as

$$I_{SFG} \propto \left|\chi^{(2)}_{eff}\right|^2 = \left|\chi^{(2)}_{NR} + \chi^{(2)}_{R}\right|^2 = \left|\chi^{(2)}_{NR} + \sum_q \frac{A_q}{\omega_{IR} - \omega_q + i\Gamma_q}\right|^2 \quad (1)$$

where $\chi^{(2)}_{NR}$, $\chi^{(2)}_{R}$, $A_q$, $\omega_q$, $\Gamma_q$ are the nonresonant and resonant contributions to $\chi^{(2)}_{eff}$, and the oscillator strength, resonant frequency and linewidth of the $q$th vibrational mode, respectively. The mode amplitude $A_q$ is proportional to the surface density of molecules and a geometrical factor representing their average orientation. Eq. (1) demonstrates a feature of nonlinear spectroscopic methods that differs from their linear counterparts: there is *interference* of the resonant contribution, $\chi^{(2)}_{R}$, with the non-resonant background from all other vibrational and electronic transitions, $\chi^{(2)}_{NR}$, leading to changes in the spectral lineshape which depend on both the magnitude and phase of $\chi^{(2)}_{NR}$, and also on the presence of nearby resonances. Therefore, a quantitative analysis of SFG spectra requires curve fitting to Eq. (1) to obtain the amplitudes, frequencies and linewidths of the resonances. Further details on the SFG technique are available in [57,58].

The SFG spectra of the carbonyl and amide groups from DDG, enzyme and chitosan were acquired with *ssp* polarization combination (*s*-polarized sum-frequency generated beam, *s*-visible beam and *p*-infrared beam). To perform SFG spectroscopy experiments *in situ*, DDG Langmuir monolayers were prepared in a KSV minimicro trough (KSV Finland) with dimensions of 195 mm × 51 mm × 4 mm. DDG was spread on subphases containing chitosan solutions at concentrations of 0.20 g $L^{-1}$ and 0.30 g $L^{-1}$. 1 mL of 0.070 g $L^{-1}$ HPL stock solution was injected behind the barrier for a monolayer at 30 mN $m^{-1}$, leading to a final concentration of 1.4 μg $mL^{-1}$, which is the same used in experiments of dynamic surface tension and PM-IRRAS.

For the transfer of Gibbs monolayers onto solid supports, two types of substrate were used: AT-cut quartz crystal, coated with Au on a 0.4 $cm^2$ active area (Stanford Research Systems, Inc.) with a fundamental frequency of *ca.* 5 MHz for quartz crystal microbalance (QCM) experiments, and silicon wafers for atomic force microscopy (AFM) analyses. The surface pressure used in the depositions was 22 mN $m^{-1}$ and the monolayer was kept at this pressure for 20 min to ensure stabilization. One-layer film was produced by removing the solid substrate from the aqueous solution, using the dipping speed of 8.0 mm $min^{-1}$, with the transfer ratio being close to 1.0. AFM analyses were obtained using a Bruker instrument, employing the tapping mode and a resonance frequency of approximately 300 kHz. The scan rate was 1 Hz and the tip was made of silicon nitride. The scales of the images were 4 $\mu m^2$.

## 3. Results and discussion

Fig. 1A shows the surface pressure-area isotherms for a DDG monolayer, featuring a minimum area ($A_{min}$) and collapse pressure of 72 $Å^2$ $molecule^{-1}$ and 41 mN $m^{-1}$, respectively, for water as subphase, consistent with the literature [59]. There is a slight increase in $A_{min}$ when water was replaced by the Theorell–Stenhagen buffer at pH = 3.0. For the range of concentrations of chitosan solutions employed, there was no significant change in surface tension, which indicates the low surface activity for chitosan. For concentrations varying from 0.05 to 0.30 g $L^{-1}$ chitosan caused a shift of the DDG surface pressure isotherms to larger areas per molecule, which means that the lipid monolayers were expanded, even

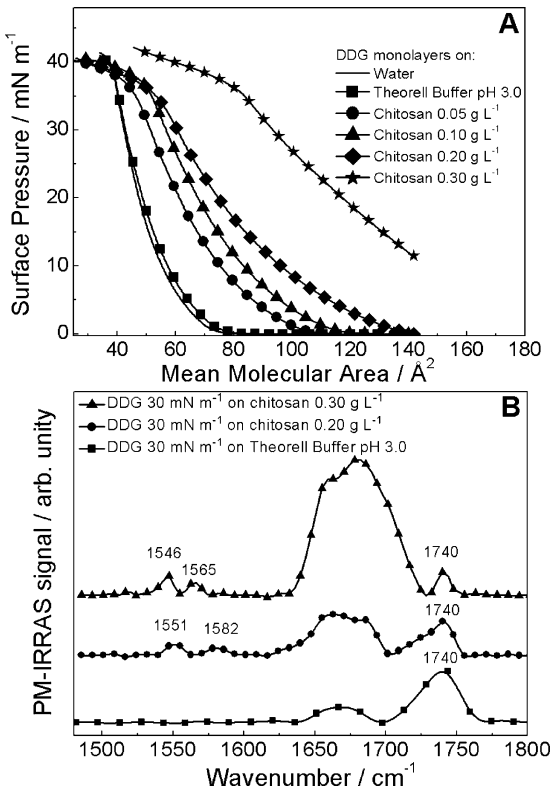


**Fig. 1.** (A) Surface pressure isotherms for DDG monolayers on different chitosan concentrations in the aqueous subphase, as indicated in the inset. In each case, isotherms were repeated three times and the standard deviations were ±1 mN $m^{-1}$. For the chitosan concentration of 0.30 g $L^{-1}$, standard deviation in surface pressure was ±1.8 mN $m^{-1}$. (B) PM-IRRA spectra in the 1500–1800 $cm^{-1}$ region for DDG monolayers at 30 mN $m^{-1}$ on: Theorell buffer pH 3.0 -■-; chitosan 0.20 g $L^{-1}$ -●- and chitosan 0.30 g $L^{-1}$ -▲-.

at high surface pressures (30–35 mN $m^{-1}$), suggesting that chitosan remains adsorbed on the packed DDG film. The surface pressure-area isotherms in Fig. 1A were obtained by spreading the DDG solution on chitosan-containing subphases and waiting for 4 h before compression started. For the chitosan concentrations up to 0.20 g $L^{-1}$ the surface pressure remained at zero, thus indicating no surface activity. In contrast, for a chitosan concentration of 0.30 g $L^{-1}$, the surface pressure increased after lipid spreading, with equilibrium reached within 10–12 h at a surface pressure of 12 mN $m^{-1}$ approximately. Therefore, surface activity was observed for this high concentration, as shown in the adsorption kinetics curve in Fig. S1 in the Supplementary Material. Accordingly, the resulting surface pressure-area isotherm for this higher chitosan concentration is more expanded.

This ability of chitosan to expand DDG monolayers is consistent with the literature, for such expansion has been observed for several surfactants, including lipids or phospholipids such as stearic acid, oleic acid, linoleic acid, α-linoleic acid, cholesterol, dipalmitoylphosphatidylglycerol (DPPG), dipalmitoylphosphatidylcholine (DPPC) and dimyristoylphosphatidic acid (DMPA) [42–44,49–51]. The maximum $C_S^{-1}$ ($C_S^{-1}{}_{max}$) can be used to characterize the surface packing of the monolayers [60]. Fig. S2 in the Supplementary Material shows the surface pressure dependence of $C_S^{-1}$ obtained from the isotherms in Fig. 1A. The DDG monolayers formed on Theorell buffer and on chitosan concentrations of 0.05 g $L^{-1}$ and 0.10 g $L^{-1}$ can be classified as liquid because $C_S^{-1}{}_{max}$ lies between 50 and 100 mN $m^{-1}$. DDG monolayers on chitosan concentrations of 0.20 g $L^{-1}$ and 0.30 g $L^{-1}$ may be classified as liquid-expanded since $C_S^{-1}{}_{max}$ varies from 30 to 50 mN $m^{-1}$. The penetration of chitosan into DDG monolayers reduces $C_S^{-1}$, making the

monolayers more flexible, similarly to what was observed for phospholipid monolayers [42,43,50,51].

In order to understand the molecular-level interactions between chitosan and DDG, PM-IRRAS experiments were carried out. Fig. S3 in the Supplementary Material shows the PM-IRRA spectra in the 2800–3000 $cm^{-1}$ region for DDG monolayers at 30 mN $m^{-1}$. The spectra for DDG monolayer without and with chitosan display two broad bands around at 2850 and 2920 $cm^{-1}$, ascribed to symmetric and asymmetric C—H stretching in $CH_2$, respectively [44,61]. What is new in the present work is the decrease in the ordering effect for the highest chitosan concentration used. Indeed, for the 0.30 g $L^{-1}$ concentration, not only surface activity was observed (see Fig. S1) but also the DDG chains became less ordered in comparison to the results for the lower chitosan concentration (0.20 g $L^{-1}$). This is inferred from the shift to larger wavenumbers of the symmetric and asymmetric $CH_2$ bands observed upon comparing the spectra for 0.20 and 0.30 g $L^{-1}$ concentrations. Czapla et al. have found a disordering effect of phospholipid monolayers upon interacting with non-steroidal antiinflamatory drugs [62]. All bands found were positive with regard to the baseline, which means that the corresponding vibration moments are oriented roughly parallel to the interface [63].

Fig. 1B shows PM-IRRA spectra in the 1500–1800 $cm^{-1}$ region for DDG monolayers at 30 mN $m^{-1}$, featuring a broad band at 1737–1741 $cm^{-1}$ due to C=O stretching vibration [61] and a strong band assigned to H—O—H bending from surface water molecules at 1650–1720 $cm^{-1}$ [61]. This latter band results from the difference in reflectivity between covered and uncovered aqueous subphases with the lipid monolayer [64]. For DDG monolayers on subphases containing chitosan, the spectra displayed two bands at 1546–1551 $cm^{-1}$ and 1565–1582 $cm^{-1}$ assigned respectively to protonated amines (—$NH_3^+$ symmetric bend) of chitosan and NH bending from the acetylated glycosamine residues (—NH—CO—) [44,65] (amide II). Therefore, these PM-IRRAS spectra confirm the presence of chitosan at the interface, as inferred from the surface pressure isotherms.

In order to probe the enzymatic activity of HPL toward hydrolysis of DDG, we first studied the surface activity of HPL. Gibbs monolayers of HPL could not be formed for concentrations below 0.80 μg $mL^{-1}$, and there was only a small concentration dependence above 2 μg $mL^{-1}$. We have therefore chosen 1.4 μg $mL^{-1}$ in the Theorell buffer for further studies. The equilibrium pressure reached was 11 ± 2 mN $m^{-1}$ and there was an induction time before the pressure started to increase significantly, as shown in Fig. 2. This equilibrium surface pressure is higher than the 7 mN $m^{-1}$ reported by de La Fournière et al. [66], for a 2.0 μg $mL^{-1}$ HPL injected into a subphase made with Tris–HCl buffer $50 \times 10^{-3}$ mol $L^{-1}$ at pH 7.4 with NaCl $150 \times 10^{-3}$ mol $L^{-1}$. Even though the HPL concentration used here was lower, the higher equilibrium surface pressure may be related to unfolding and/or change in conformation of HPL, that is more pronounced in acidic than in neutral media. Proteins adsorbed at air–liquid interfaces can expose hydrophobic parts causing partial unfolding or undergo modification in polypeptide conformation. This has already been studied for β casein, bovine serum albumin, lysozyme and ovalbumine [67–69]. Ranaldi et al. [54] investigated structural changes of HPL in acidic conditions by attenuated total reflectance Fourier transform infrared spectroscopy and electron paramagnetic resonance spectroscopy, and concluded that for pH 6.5–3.0 the secondary structure of HPL is maintained, while at pH below 3.0 HPL is completely unfolded with irreversible loss of the enzymatic activity.

Fig. 2A also shows that when the subphase contained 0.20 g $L^{-1}$ chitosan, the induction time was shorter but the maximum pressure reached was the same. If the chitosan concentration was 0.30 g $L^{-1}$, then there was practically no induction time and the equilibrium surface pressure increased to 18 ± 2 mN $m^{-1}$. This

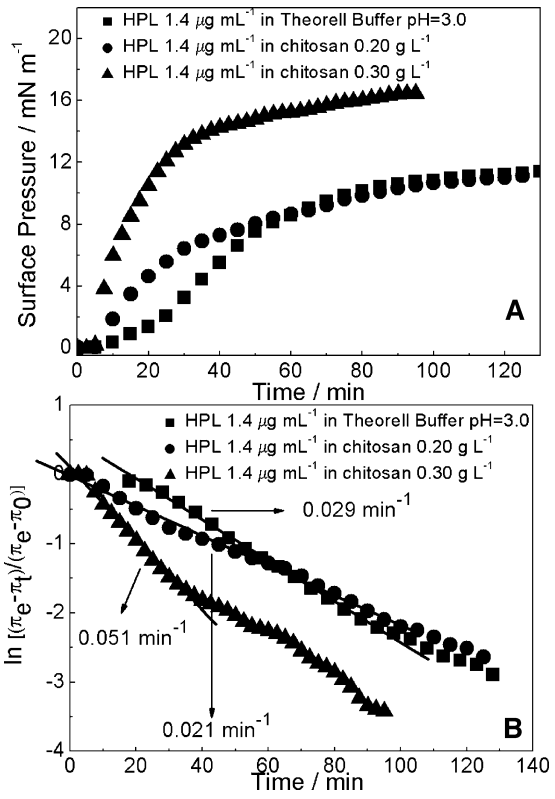


**Fig. 2.** (A) Adsorption kinetics for HPL 1.4 μg $mL^{-1}$ injected into various subphase solutions: Theorell buffer pH 3.0 ■; chitosan 0.20 g $L^{-1}$ ● and chitosan 0.30 g $L^{-1}$ ▲. In each case, the curve was repeated three times and the standard deviation was ±2 mN $m^{-1}$. (B) First-order rate constants extracted from the curves of adsorption kinetics in 2 A.

increase can be related to the formation of a complex between HPL and chitosan, even though both compounds have positive charges under the experimental conditions used since the isoelectric point of HPL is 5.4 [70]. This interaction between chitosan and HPL is probably dominated by hydrophobic interactions and/or hydrogen bonding. Chen and Tianqing reported complex formation between positively charged hemoglobin and chitosan owing to hydrogen bonding/hydrophobic interactions with modification of hemoglobin conformation [71]. Complex formation has also been found between chitosan and porcine gastric mucin (PGM) [72], which was attributed to electrostatic interactions, with chitosan increasing the surface activity of PGM. For β-lactoglobulin, on the other hand, surface activity was actually decreased by chitosan that even removed protein molecules from the phospholipid monolayer [63].

The adsorption kinetics curves in Fig. 2A can be treated quantitatively using the approach suggested by Maget-Dana [73,74], where a first-order equation is applied. Formally, $\ln[(\pi_e - \pi_t) - (\pi_e - \pi_0)] = -kt$, where $\pi_e$, $\pi_t$ and $\pi_0$ are the surface pressures at equilibrium, time $t$ and initial time, respectively, and $k$ is the rate constant. The $k$ values are related to protein adsorption and/or penetration and they were extracted from fitting the initial change in the surface pressure curves, as indicated in Fig. 2B. For the data in pure Theorell buffer, the kinetic behavior was different and we neglected the initial lag time to extract the rate constant. The values for k were 0.029 $min^{-1}$, 0.021 $min^{-1}$ and 0.051 $min^{-1}$ respectively, for adsorption of HPL in Theorell buffer, chitosan 0.20 g $L^{-1}$ and chitosan 0.30 g $L^{-1}$, being similar to those for proteins such as β-lactoglobulin and bovine serum albumin adsorbed on a phosphate buffer solution [75]. We have explored only the rate constant for the initial adsorption/penetration process because an

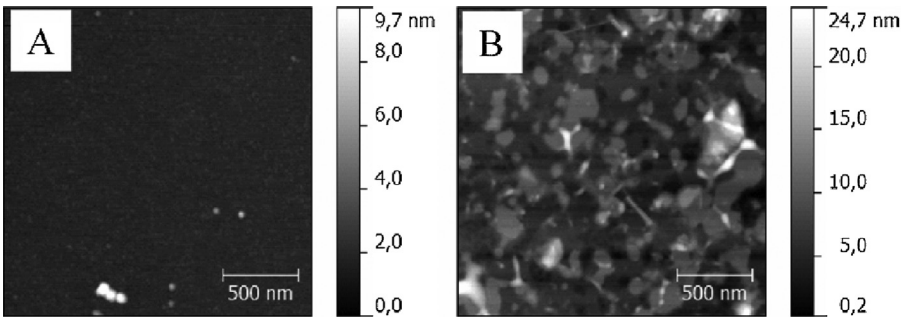


**Fig. 3.** AFM images of Gibbs films with one layer of: HPL (A) and complex between HPL and chitosan (B).

eventual interfacial rearrangement (second step) is masked in our measurements by subphase evaporation, which affects the reading of surface pressure at long times.

To investigate morphology of the interface formed by HPL and by the complex between HPL and chitosan, the Gibbs monolayer was transferred onto silicon wafers using the vertical deposition method as for Langmuir–Blodgett films. The AFM images of one-layer films in Fig. 3 display homogeneous morphology for the HPL film, while the film containing the HPL + chitosan complex contains aggregates distributed all over, as indicated in Fig. 3B. The transfer of HPL + chitosan led to a larger mass for the solid film. According to the QCM data, a mass of 6.81 ng was transferred for the HPL + chitosan film, in comparison to 4.24 ng for the film containing only HPL.

Fig. S4 in the Supplementary Material shows the PM-IRRA spectra for DDG monolayers at 30 mN $m^{-1}$, without and with the presence of chitosan in the subphase, before and after injecting HPL into the subphase. HPL injection causes the opening of the barriers to maintain the surface pressure constant at 30 mN $m^{-1}$, as result of the penetration/adsorption of HPL in the DDG monolayer. When HPL was injected in the monolayer without chitosan, two bands appeared which are due to proteins, as follows. The amide II band at 1540 $cm^{-1}$ is ascribed to the in-plane bending of NH and CN stretching, while the amide I band at 1620 $cm^{-1}$ is assigned to C=O stretching vibrations from polypeptides. The band at 1670 $cm^{-1}$ is attributed to the difference in reflectivity between covered and uncovered surfaces as described before. After 4 h of hydrolysis, the intensity of the C=O stretching band from DDG at 1740 $cm^{-1}$ decreased more clearly in figures S4A and S4B than in S4C, because of the intense band of water. When chitosan was present in the subphase, specific bands from HPL cannot be identified because amide II and amide I regions are superimposed by bands from chitosan and water, respectively.

Even though a decrease in the intensities of the C=O stretching bands from DDG can be noted, an estimation of the hydrolysis is not possible because the baselines of the spectra were adjusted. Such procedure could lead to unreliable values of DDG degradation if, for example, the integration of the bands were made. A detailed estimation of DDG hydrolysis was performed by SFG spectroscopy as described below.

DDG hydrolysis was explored using SFG spectroscopy, similarly to the work by Niaura et al. [76]. Fig. 4 shows SFG spectra in the 1600–1800 $cm^{-1}$ region for the three systems studied here. In all cases before HPL injection, carbonyl stretching bands from DDG are intense and broad within 1700–1770 $cm^{-1}$, and could be better defined by fitting the experimental data to Eq. (1) [77]. The broad carbonyl band comprises two main peaks centered at *ca.* 1712 $cm^{-1}$ and 1732 $cm^{-1}$, assigned to the double- and single-hydrogen bonded carbonyl stretching vibrations of DDG, respectively [78]. Fig. 5A shows typical fitting of one experimental spectrum before HPL injection, highlighting the two main bands and the accuracy of the fitting. Since the C=O groups of DDG are not so close to each other, probably their vibrations are not coupled, which gives rise to the observed single C=O peak. Otherwise, if the coupling were strong, it would lead to two peaks from symmetric and asymmetric stretching [79,80]. One should note that before HPL injection, the spectra in Fig 4B and C, with chitosan in the subphase, no additional signal was observed other than those assigned to DDG. After 4 h of HPL injection, all systems presented a decreased intensity of the carbonyl peak. This is observed by comparing with the initial spectra (before enzyme injection) in Fig. 4.

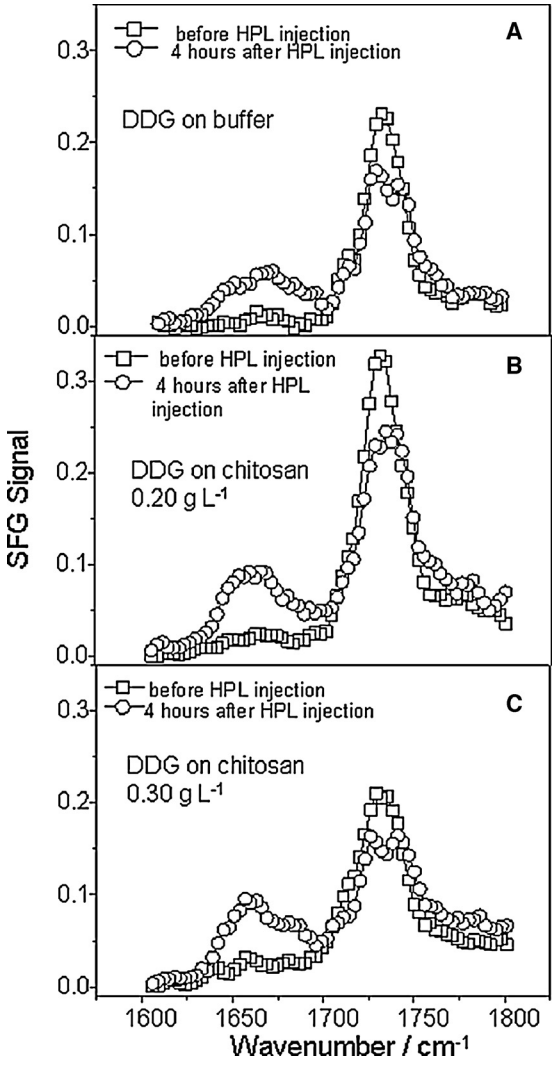


**Fig. 4.** SFG spectra for DDG monolayers at 30 mN $m^{-1}$ before the HPL injection (-□-), and 4 h after of HPL injection (-○-). The graphs show the measurements for DDG on (A) Theorell buffer, (B) chitosan 0.20 g $L^{-1}$ and (C) chitosan 0.30 g $L^{-1}$.

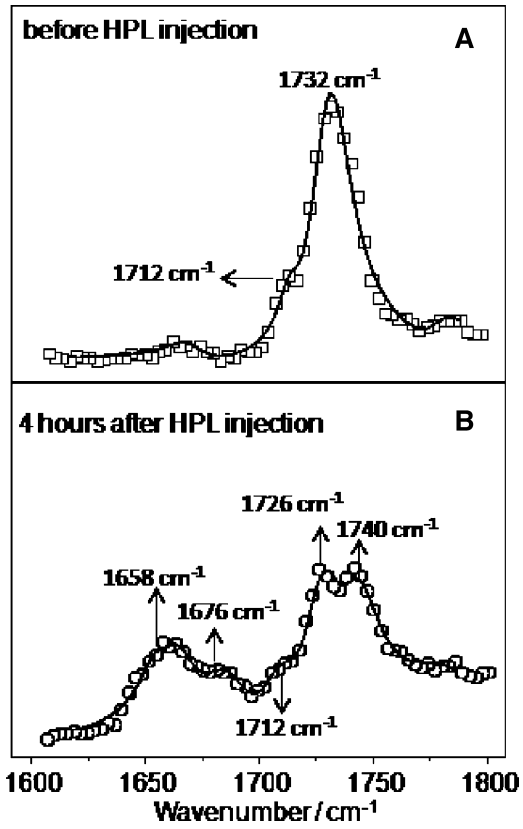


**Fig. 5.** SFG spectra for DDG monolayers on Theorell buffer pH 3.0 at 30 mN m$^{-1}$ (A) before HPL injection and (B) 4 h after HPL injection. Before the enzyme injection, the carbonyl group from DDG presents two peaks at 1712 and 1732 cm$^{-1}$, and 4 h after the enzyme hydrolyzing the more intense peak is split into two bands at *ca.* 1727 and 1740 cm$^{-1}$. In (B) it is also possible to check the enzyme bands at 1658 and 1676 cm$^{-1}$ revealing that HPL most predominant structure is α-helix.

Therefore, one concludes that chitosan did not block enzyme action for hydrolyzing DDG at any of the chitosan concentrations studied here.

In order to quantify the extent of DDG hydrolysis from the SFG spectra, it is necessary to fit the carbonyl bands before and after 4 h of HPL injection and analyze the extracted mode amplitudes. The spectral characteristics (peak position, strength and band width) were obtained by nonlinear curve-fitting to Eq. (1) for measurements before HPL injection, 2 h and 4 h after enzyme injection. Fig. 5B shows an experimental spectrum of DDG after 4 h of HPL injection fitted by five peaks, and these peaks could be assigned to HPL or DDG. The fitting parameters are displayed in Table 1. The peaks assigned to the carbonyl stretch are centered at *ca.* 1712, 1727 and 1740 cm$^{-1}$. The carbonyl peak of DDG at 1712 cm$^{-1}$ remained constant, while the peak centered at ~ 1730 cm$^{-1}$ was considerably reduced, and a new component appeared at 1740 cm$^{-1}$. All these changes could be associated with the presence of the enzyme and the hydrolysis process [76,81,82]. The frequency of the C=O vibrational mode is known to be very sensitive to the environment, especially to hydrogen-bonding interactions; for instance, the C=O stretching bands for fatty acids at the air–water interface shift from 1740 cm$^{-1}$ to 1702 cm$^{-1}$ if they are non-hydrogen-bonded, singly hydrogen-bonded or doubly hydrogen-bonded, respectively [81,83–85]. Assuming that the non-hydrogen-bonded C=O is assigned to the free fatty acid resulting from DDG hydrolysis (presumably because its interaction with water is shielded by the enzyme or the bulky DDG headgroup), which stays within the monolayer, we can quantify the enzyme activity from the amplitudes of C=O components in the SFG spectra. It should be noted that at first it may seem unlikely that decanoic acid would still remain in the monolayer, since its solubility in water is appreciable, around 30 mg L$^{-1}$. However, at low pH the acid group is protonated, reducing its solubility. Furthermore, the fatty acid is generated already incorporated within a Langmuir film, and its solubilization in water would involve breaking its interaction with the nearby alkyl chains in the film, leading to a significant energy barrier for solubilization. Indeed, the expansion of the monolayer after HPL injection (due to the enzyme incorporation in the film) is not followed by a barrier contraction at longer times, which would be expected if the product of DDG hydrolysis were soluble in the subphase. Therefore, this observation further supports our assignment of the non-hydrogen-bonded C=O component at 1740 cm$^{-1}$ to protonated fatty acids resulting from DDG hydrolysis that remain in the Langmuir film, while the singly- and doubly-hydrogen-bonded C=O (~1730 and 1712 cm$^{-1}$ respectively) are attributed to DDG.

The amplitude at 1712 cm$^{-1}$ in Table 1 is the same for all periods and systems studied. Hence, we may conclude that doubly-hydrogen bonded C=O of DDG is not significantly affected by enzymatic hydrolysis up to 4 h, with fluctuations for the values nearly within the fitting uncertainties. However, the strength for the peak at 1740 cm$^{-1}$ (representing the free fatty acid) increases with time, and we can quantify the hydrolyzed fraction of DDG by the reduction in the combined amplitudes of DDG C=O modes (sum of amplitudes at 1730 and 1712 cm$^{-1}$). For DDG on Theorell buffer, the hydrolyzed fraction after 4 h is about 33%, while on the subphase containing 0.20 g L$^{-1}$ of chitosan it increases to 50%, and with chitosan concentration of 0.30 g L$^{-1}$ the hydrolyzed fraction is again about 29%. These estimates are consistent with the relative

**Table 1**
Fitting parameters of the SFG spectra.

| | DDG on Theorell buffer pH 3.0 | | DDG on chitosan (0.20 g L$^{-1}$) | | DDG on chitosan (0.30 g L$^{-1}$) | |
|---|---|---|---|---|---|---|
| | Strength ($A$) | Width ($\Gamma$, cm$^{-1}$) | Strength ($A$) | Width ($\Gamma$, cm$^{-1}$) | Strength ($A$) | Width ($\Gamma$, cm$^{-1}$) |
| *Before HPL injection* | | | | | | |
| 1712 cm$^{-1}$ | *0.5* ± 0.1 | *6.1* ± 0.5 | *1.0* ± 0.1 | *10.2* ± 1.6 | *1.4* ± 0.1 | *10.5* ± 1.7 |
| 1734 cm$^{-1}$ | *5.7* ± 0.2 | *11.1* ± 1.6 | *6.7* ± 0.2 | *12.3* ± 1.2 | *5.8* ± 0.1 | *12.1* ± 1.3 |
| *2 h after HPL injection* | | | | | | |
| 1712 cm$^{-1}$ | *0.7* ± 0.1 | *6.1* ± 0.6 | *1.2* ± 0.1 | *10.4* ± 1.2 | *1.8* ± 0.2 | *10.8* ± 1.2 |
| 1727 cm$^{-1}$ | *3.1* ± 0.2 | *10.1* ± 1.6 | *3.1* ± 0.2 | *10.9* ± 1.5 | *3.3* ± 0.2 | *11.0* ± 1.7 |
| 1740 cm$^{-1}$ | *1.2* ± 0.1 | *7.5* ± 1.0 | *2.0* ± 0.2 | *8.9* ± 1.3 | *1.3* ± 0.1 | *7.0* ± 0.8 |
| *4 h after HPL injection* | | | | | | |
| 1712 cm$^{-1}$ | 0.7 ± 0.1 | 6.0 ± 0.5 | 1.3 ± 0.2 | 10.3 ± 1.4 | 1.8 ± 0.2 | 10.8 ± 1.3 |
| 1727 cm$^{-1}$ | 3.5 ± 0.2 | 10.1 ± 1.5 | 2.5 ± 0.2 | 10.9 ± 1.6 | 3.3 ± 0.2 | 11.1 ± 1.9 |
| 1740 cm$^{-1}$ | 1.5 ± 0.1 | 7.5 ± 0.9 | 2.6 ± 0.2 | 8.9 ± 1.0 | 1.5 ± 0.1 | 7.2 ± 0.8 |

The error bars were obtained by the nonlinear least-squares fitting algorithm (Levenberg–Marquardt, as implemented in Origin 8.0). They represent the uncertainty in the best fit values for peak parameters strength and width. The spectrum submitted for fitting analysis is an arithmetic mean of three experimental curves, so that it represents a characteristic behavior of the system under investigation. Investigations were repeated in different days, and nearly identical spectra were obtained.

amplitudes 4 h after HPL injection in the three subphases, since the value on the subphase with 0.20 g $L^{-1}$ of chitosan is about 5/3 larger than on pure buffer or on the subphase with 0.30 g $L^{-1}$ of chitosan. It is also interesting to note that the mode amplitudes (and therefore the calculated hydrolyzed fraction of DDG) are not very different after 2 h or 4 h of HPL injection, indicating that the enzyme loses activity in such a timeframe. This is in agreement with the observations in Ref. [54], where HPL was shown to lose a vast majority of its activity over a 4 h period at pH 3.

Another important observation is the appearance of two peaks at *ca.* 1658 $cm^{-1}$ and 1676 $cm^{-1}$ for the spectrum obtained 4 h after enzyme injection in Fig. 5B, which are assigned to amide I of HPL. Therefore, even though HPL was injected in the subphase, it went to the interface and took a preferential orientation, with the peak position of the amide I band indicating that the enzyme predominantly adopts α-helix and turns structures during its action in hydrolyzing DDG [86,87].

The work presented here contradicts a study involving the influence of chitosan on enzymatic activity of porcine pancreatic lipase [88]. The quantity of fatty acid released in corn oil-in-water emulsion at pH 7 containing lecithin and chitosan was smaller than without chitosan because fat was captured by chitosan, thus blocking the enzyme access. One should stress, however, that the experimental conditions differed markedly. While in Ref. [88] chitosan was acting in an environment with oil emulsion in water, here we used a Langmuir monolayer at the air/water interface with subphase solution under acidic conditions.

## 4. Conclusion

With the main aim of understanding how chitosan could affect the action of HPL toward DDG, we first investigated molecular-level interactions between chitosan and DDG, where chitosan was found to adsorb on and expand DDG Langmuir monolayers even at high surface pressures. According to the PM-IRRAS experiments, the interactions between chitosan and DDG included hydrophobic interactions. Also from the PM-IRRAS data we could infer that chitosan at concentration of 0.20 g $L^{-1}$ induced ordering of the DDG alkyl chains. This effect decreased for the highest concentration of chitosan used (0.30 g $L^{-1}$), owing to the considerably larger expansion induced in the DDG monolayer.

The surface activity of HPL, which forms Gibbs monolayers at the air/water interface, is significantly affected by chitosan, especially at the higher chitosan concentrations. An increased surface activity was attributed to complex formation between HPL and chitosan, probably owing to H-bonding and hydrophobic interactions since both molecules are positively charged. In spite of this large effect on HPL surface activity, chitosan did not inhibit the enzymatic action of HPL toward DDG. In order to draw such conclusion, which was the primary aim in the study, we employed SFG spectroscopy. The HPL active site was not blocked by chitosan, and the enzymatic activity did not decrease when chitosan was present. The extent of DDG hydrolysis varied within the experimental error for HPL in the presence and absence of chitosan, and if there is an effect, it would be a slight increase in activity caused by chitosan.

One important implication of our findings is that – in case chitosan is proven as efficient for fat reduction – the mechanism for its action is not the blocking of HPL activity. Other mechanisms would have to be probed, including possible effects from other lipases, specific colipases, phospholipases and bile salts.

## Acknowledgements

The authors are grateful to CNPq, FAPESP and nBioNet Network (CAPES, Brazil) for the financial support. ALS thanks CNPq for his PNPD postdoctoral fellowship.

## Appendix A. Supplementary data

Supplementary data associated with this article can be found, in the online version, at http://dx.doi.org/10.1016/j.colsurfb.2014.10.040.

## References

[1] F.J. Pavinatto, L. Caseli, O.N. Oliveira Jr., Biomacromolecules 11 (2010) 1897.
[2] S.S. Koide, Nutr. Res. 18 (1998) 1091.
[3] R. Jayakumar, M. Prabaharan, P.T. Sudhessh Kumar, S.V. Nair, H. Tamura, Biotechnol. Adv. 29 (2011) 322.
[4] K. Kurita, Mar. Biotechnol. 8 (2006) 203.
[5] M.N.V. Ravi Kumar, React. Funct. Polym. 46 (2000) 1.
[6] B. Krajewska, Sep. Purif. Technol. 41 (2005) 305.
[7] F.H. Liao, M.J. Shieh, N.C. Chang, Y.W. Chien, Nutr. Res. 27 (2007) 146.
[8] C. Ni Mhurchu, C. Dunshea-Mooij, D. Bennett, A. Rodgers, Obes. Rev. 6 (2005) 35.
[9] R. Guerciolini, L. Radu-Radulescu, M. Boldrin, J. Dallas, R. Moore, Obes. Res. 9 (2001) 364.
[10] M.D. Gades, J.S. Stern, Int. J. Obes. 26 (2002) 119.
[11] G.Y. Park, S. Mun, Y. Park, S. Rhee, E.A. Decker, J. Weiss, D. Julian McClements, Y. Park, Food Chem. 104 (2007) 761.
[12] M.T. Gades, J.S. Stern, J. Am. Diet. Assoc. 105 (2005) 72.
[13] D.E. Woodgate, J.A. Conquer, Curr. Ther. Res. 64 (2003) 248.
[14] M. Sumiyoshi, Y. Kimura, J. Pharm. Pharmacol. 58 (2006) 201.
[15] M. Yuji, T. Keisuke, N. Yasue, K. Yoshiyuki, A. Makoto, T. Takashi, T. Wataru, T. Atsushi, H. Hiroyoshi, M. Tomotari, Biosci. Biotechnol. Biochem. 57 (9) (1993) 1439.
[16] R.A.A. Muzzarelli, W. Xia, M. Tomasetti, P. Ilari, Enzyme Microb. Technol. 17 (1995) 541.
[17] J.L. Nauss, J.L. Thompson, J. Nagyvary, Lipids 18 (1983) 714.
[18] P. Faldt, B. Bergenstahl, P.M. Claesson, Colloids Surf. A 71 (1993) 187.
[19] P. Reis, K. Holmberg, H. Waltzke, M.E. Leser, R. Miller, Adv. Colloid Interface Sci. 147–148 (2009) 237.
[20] P.J. Wilde, B.S. Chu, Adv. Colloid Interface Sci. 165 (2011) 14.
[21] V. Delorme, R. Dhouib, S. Canaan, S. Fotiadu, F. Carrière, J.F. Cavalier, Pharm. Res. 28 (2011) 1831.
[22] A. Torcello-Gómez, J. Maldonado-Valderrama, J. De Vicente, M.A. Cabrerizo-Vílchez, M.J. Gálvez-Ruiz, A. Martín-Rodríguez, Food Hydrocoll. 25 (2011) 809.
[23] J. Maldonado-Valderrama, P. Wilde, A. Macierzanka, A. Mackie, Adv. Colloid Interface Sci. 165 (2011) 36.
[24] A. Tiss, H. Lengsfeld, F. Carrière, R. Verger, J. Mol. Catal. B: Enzym. 58 (2009) 41.
[25] A. Tiss, H. Lengsfeld, R. Verger, J. Mol. Catal. B: Enzym. 62 (2010) 19.
[26] T. Tsujita, H. Takaichi, T. Takaku, S. Aoyama, J. Hiraki, J. Lipid Res. 47 (2006) 1852.
[27] K.A. Grove, S. Sae-tan, M.J. Kennett, J.D. Lambert, Obesity 20 (2012) 2311.
[28] B.S. Chu, G.T. Rich, M.J. Ridout, R.M. Faulks, M.S.J. Wickham, P.J. Wilde, Langmuir 25 (16) (2009) 9352.
[29] B.S. Chu, A.P. Gunning, G.T. Rich, M.J. Ridout, R.M. Faulks, M.S.J. Wickham, V.J. Morris, P.J. Wilde, Langmuir 26 (12) (2010) 9782.
[30] V. Constantinou-Kokotou, V. Magrioti, R. Verger, Chem. Eur. J. 10 (2004) 1133.
[31] G. Piéroni, Y. Gargouri, L. Sarda, R. Verger, Adv. Colloid Interface Sci. 32 (1990) 341.
[32] R. Verger, G.H. de Hass, Chem. Phys. Lipids 10 (1973) 127.
[33] M. Méthot, E. Demers, S. Bussières, B. Desbat, R. Breton, C. Salesse, Colloids Surf. A 321 (2008) 147.
[34] S. Bussières, T. Buffeteau, B. Desbat, R. Breton, C. Salesse, Biochim. Biophys. Acta 1778 (2008) 1324.
[35] I. Estrela-Lopis, G. Brezesinski, H. Mohwald, Phys. Chem. Chem. Phys. 2 (2000) 4600.
[36] I. Estrela-Lopis, G. Brezesinski, H. Mohwald, Biophys. J. 80 (2001) 749.
[37] X. Wang, S. Zheng, Q. He, G. Brezesinski, H. Mohwald, J. Li, Langmuir 21 (2005) 1051.
[38] K. Ariga, Q. Ji, T. Mori, M. Naito, Y. Yamauche, H. Abe, J.P. Hill, Chem. Soc. Rev. 42 (2013) 6322.
[39] C. Chen, Q. Xie, D. Yang, H. Xiao, Y. Fu, Y. Tan, S. Yao, RSC Adv. 3 (2013) 4473.
[40] K. Ariga, Y. Yamauchi, T. Mori, J.P. Hill, Adv. Mater. 25 (2013) 6477.
[41] K. Ariga, T. Mori, S. Ishihara, K. Kowakami, J.P. Hill, Chem. Mater. 26 (2014) 519.
[42] F.J. Pavinatto, L. Caseli, A. Pavinatto, D.S. dos Santos Jr., T.M. Nobre, M.E.D. Zaniquelli, H.S. Silva, P.B. Miranda, O.N. Oliveira Jr., Langmuir 23 (2007) 7666.
[43] F.J. Pavinatto, A. Pavinatto, L. Caseli, D.S. dos Santos Jr., T.M. Nobre, M.E.D. Zaniquelli, O.N. Oliveira Jr., Biomacromolecules 8 (2007) 1633.
[44] F.J. Pavinatto, C.P. Pacholatti, E.A. Montanha, L. Caseli, H.S. Silva, P.B. Miranda, T. Viitala, O.N. Oliveira Jr., Langmuir 25 (17) (2009) 10051.
[45] A. Pavinatto, F.J. Pavinatto, J.A.M. Delezuk, T.M. Nobre, A.L. Souza, S.P. Campana-Filho, O.N. Oliveira Jr., Colloids Surf. B (2013) 48.
[46] B. Krajewska, P. Wydro, A. Kyziol, Colloids Surf. A (2013) 349.
[47] B. Krajewska, A. Kyziol, P. Wydro, Colloids Surf. A 434 (2013) 359.
[48] Y. Wang, Y. Tang, Z. Zhou, E. Ji, G. Lopez, E. Chi, K.S. Schanze, D.G. Whitten, Langmuir 26 (15) (2010) 12509.
[49] H. Parra-Barraza, M.G. Burboa, M. Sánchez-Vásquez, J. Juárez, F.M. Goycoolea, M.A. Valdez, Biomacromolecules 6 (2005) 2416.

[50] P. Wydro, B. Krajewska, K. Hac-Wydro, Biomacromolecules 8 (2007) 2611.
[51] B. Krajewska, P. Wydro, A. Janczyk, Biomacromolecules 12 (2011) 4144.
[52] A. Pavinatto, F.J. Pavinatto, A. Barros-Timmons, O.N. Oliveira Jr., ACS Appl. Mater. Interfaces 2 (1) (2010) 246.
[53] A. Pavinatto, A.L. Souza, J.A.M. Delezuk, F.J. Pavinatto, S.P. Campana-Filho, O.N. Oliveira Jr., Colloids Surf. B 114 (2014) 53.
[54] S. Ranaldi, V. Belle, M. Wouldstra, J. Rodriguez, B. Guigliarelli, J. Sturgis, F. Carriere, A. Fournel, Biochemistry 48 (2009) 630.
[55] S. Di Maio, R.L. Carrier, J. Control. Release 151 (2011) 110.
[56] P.B. Miranda, V. Pflumio, H. Saijo, Y.R. Shen, Thin Solid Films 327–329 (1998) 161.
[57] Y.R. Shen, Surf. Sci. (1994) 299–300, 551.
[58] A.G. Lambert, P.B. Davies, D.J. Neivandt, Appl. Spectrosc. Rev. 40 (2005) 103.
[59] E. Rogalska, S. Nury, I. Douchet, R. Verger, Chirality 7 (1995) 505.
[60] J.T. Davies, E.K. Rideal, Interfacial Phenomena, Academic Press, New York, 1963.
[61] A. Dicko, H. Bourque, M. Pézolet, Chem. Phys. Lipids 96 (1998) 125.
[62] K. Czapla, B. Korchowiec, E. Rogalska, Langmuir 26 (2010) 3485.
[63] L. Caseli, F.J. Pavinatto, T.M. Nobre, M.E.D. Zaniquelli, T. Viitala, O.N. Oliveira Jr., Langmuir 24 (8) (2008) 4150.
[64] D. Blaudez, T. Buffeteau, J.C. Cornut, D. Desbat, N. Escrafe, M. Pezolet, J.M. Turlet, Appl. Spectrosc. 47 (1993) 869.
[65] G. Lawrie, I. Keen, B. Drew, A. Chandler-Temple, L. Rintoul, P. Fredericks, L. Grondahl, Biomacromolecules 8 (2001) 2533.
[66] L. de La Fournière, M.G. Ivanova, J.P. Blond, F. Carrière, R. Verger, Colloids Surf. B (1994) 585.
[67] D.E. Graham, M.C. Phillips, J. Colloid Interface Sci. 70 (3) (1979) 427.
[68] C. Ybert, J.M. di Meglio, Langmuir 14 (1998) 471.
[69] R. Miller, V.B. Fainerman, A.V. Makievski, J. Kragel, D.O. Grigoriev, V.N. Kazakov, O.V. Sinyachenko, Adv. Colloid Interface Sci. 86 (2000) 39.
[70] A. De Caro, C. Figarella, J. Amic, R. Michel, O. Guy, Biochim. Biophys. Acta 490 (2) (1977) 411.
[71] L. Chen, T. Tianqing, Int. J. Biol. Macromol. 42 (2008) 441.
[72] C.A. Silva, T.M. Nobre, F.J. Pavinatto, O.N. Oliveira Jr., J. Colloid Interface Sci. 376 (2012) 289.
[73] R. Maget-Dana, M. Ptak, Colloids Surf. B 7 (1996) 135.
[74] R. Maget-Dana, Biochim. Biophys. Acta 1462 (1999) 109.
[75] P. Suttiprasit, V. Krisdhasima, J. Mcguire, J. Colloid Interface Sci. 154 (1992) 316.
[76] G. Niaura, Z. Kuprionis, I. Ignatjev, M. Kazemekaite, G. Valincius, Z. Talaikyte, V. Razumas, A. Svendsen, J. Phys. Chem. B 112 (2008) 4094.
[77] X. Zhuang, P.B. Miranda, D. Kim, Y.R. Shen, Phys. Rev. B: Condens. Matter Mater. Phys. 59 (1999) 12632.
[78] J. Jay Leitch, C.L. Brosseau, S.G. Roscoe, K. Bessonov, J.R. Dutcher, J. Lipkowski, Langmuir 29 (2013) 965.
[79] X. Bin, I. Zawisza, J.D. Goddard, J. Lipkowski, Langmuir 21 (2005) 330.
[80] L.J. Bellamy, The Infrared Spectra of Complex Molecules: Advances in Infrared Group Frequencies, vol. 2, 2nd ed., Chapman & Hall Press, London, 1980.
[81] C. Santambrogio, F. Sasso, A. Natalello, S. Brocca, R. Grandori, S.M. Doglia, M. Lotti, Appl. Microbiol. Biotechnol. 97 (2013) 8609.
[82] A. Natalello, F. Sasso, F. Secundo, Biotechnol. J. 8 (2013) 133.
[83] A. Gericke, H. Huhnerfuss, J. Phys. Chem. 97 (1993) 12899.
[84] R. Johann, D. Vollhardt, H. Mohwald, Colloids Surf. A (2001) 311.
[85] R.N.A.H. Lewis, R.N. McElhaney, Chem. Phys. Lipids 96 (1998) 9.
[86] F.C. Rinaldi, A.N. Meza, B.G. Guimarães, Biochemistry 48 (2009) 3508.
[87] A. Natalello, D. Ami, S. Brocca, M. Lotti, S.M. Doglia, Biochem. J. 385 (2005) 511.
[88] S. Mun, E.A. Decker, Y. Park, J. Weiss, D.J. McClements, Food Biophys. 1 (2006) 21–29.